Renewable Energy 80 (2015) 724–736

Contents lists available at ScienceDirect

Renewable Energy

journal homepage: www.elsevier.com/locate/renene

Foundation damping and the dynamics of offshore wind turbine monopiles

W. Carswell [a, *], J. Johansson [b], F. Løvholt [b], S.R. Arwade [a], C. Madshus [b], D.J. DeGroot [a], A.T. Myers [c]

[a] Department of Civil & Environmental Engineering, University of Massachusetts – Amherst, 130 Natural Resources Road, Amherst, MA 01003, USA
[b] Norwegian Geotechnical Institute, Sognsveien 72, 0855 Oslo, Norway
[c] Department of Civil & Environmental Engineering, Northeastern University, Boston, MA 02115, USA

ARTICLE INFO

Article history:
Received 15 July 2014
Accepted 23 February 2015
Available online 19 March 2015

Keywords:
Offshore wind turbine
Monopile
Soil-structure interaction
Damping

ABSTRACT

The contribution of foundation damping to offshore wind turbines (OWTs) is not well known, though researchers have back-calculated foundation damping from "rotor-stop" tests after estimating aerodynamic, hydrodynamic, and structural damping with numerical models. Because design guidelines do not currently recommend methods for determining foundation damping, it is typically neglected. This paper investigates the significance of foundation damping on monopile-supported OWTs subjected to extreme storm loading using a linear elastic two-dimensional finite element model. The effect of foundation damping primarily on the first natural frequency of the OWT was considered as OWT behavior is dominated by the first mode under storm loading. A simplified foundation model based on the soil-pile mudline stiffness matrix was used to represent the monopile, hydrodynamic effects were modeled via added hydrodynamic mass, and 1.00% Rayleigh structural damping was assumed. Hysteretic energy loss in the foundation was converted into a viscous, rotational dashpot at the mudline to represent foundation damping. Using the logarithmic decrement method on a finite element free vibration time history, 0.17%-0.28% of critical damping was attributed to foundation damping. Stochastic time history analysis of extreme storm conditions indicated that mudline OWT foundation damping decreases the maximum and standard deviation of mudline moment by 7–9%.

1. Introduction

Economics are a major impediment for utility-scale offshore wind installations. Offshore wind farms require large capital investments and can have approximately two to three times the operation and management costs as compared to onshore wind [1]; however, due to higher, more consistent wind speeds, offshore wind farms can offer more renewable energy than their onshore counterparts and it is expected that monopile foundations will continue to have a large market share despite some increase in deployment of larger turbines at greater water depths [2]. For monopiles in deeper water, the dynamic effect of wave loads becomes a design driver for OWT support structures, leading to an increased sensitivity to soil stiffness and damping [2]. Higher damping in the support structure can lead to lower design load estimates, which in turn can correspond to reduced amounts of material required to resist loading. Because support structures contribute approximately 20–25% of the capital cost for OWTs [1,3], it is imperative to identify and assess sources of damping in the effort to improve the economics of offshore wind energy.

Sources of damping for OWTs include aerodynamic, hydrodynamic, structural, and soil damping. In addition, for some turbines, tuned mass dampers are also installed in the nacelle. Aerodynamic damping occurs when the OWT blades respond to increases and decreases in aerodynamic force due to the relative wind speed from tower top motion [4,5]. During power production, aerodynamic damping is a dominant source of damping in the fore-aft direction; however, aerodynamic damping is far less significant in the fore-aft direction for parked and feathered rotors or in the side-to-side direction for design situations including wind-wave misalignment [5–7]. During design situations such as these, other sources of damping play a much larger role in the dynamics of the structure.

* Corresponding author. Tel.: +1 413 545 0686.
E-mail addresses: wcarswel@umass.edu (W. Carswell), jorgen.johansson@ngi.no (J. Johansson), finn.lovholt@ngi.no (F. Løvholt), arwade@umass.edu (S.R. Arwade), christian.madshus@ngi.no (C. Madshus), degroot@umass.edu (D.J. DeGroot), atm@neu.edu (A.T. Myers).

http://dx.doi.org/10.1016/j.renene.2015.02.058
0960-1481/

Nomenclature

A	amplitude
$c_{\theta\theta}$	rotational damping constant
C_m	inertia coefficient
C_D	drag coefficient
D	damping factor
E_h	hysteretic energy loss
f	frequency
G	shear modulus
H_x	horizontal mudline shear
k	mudline spring stiffness
k'	decoupled spring stiffness
k_{mud}	mudline stiffness matrix
L_{eq}	rigid decoupling length
M_ϕ	mudline moment
n	number of amplitudes
s_u	undrained shear strength
u	mudline displacement
u_{top}	tower top displacement
x	horizontal translation degree of freedom
α	Rayleigh mass coefficient
β	Rayleigh stiffness coefficient
δ	log decrement
η	loss factor
ϕ	rotational degree of freedom
θ	mudline rotation
μ	mean
ν	Poisson's ratio
σ	standard deviation
ξ	critical damping ratio
ω_n	frequency (rad/s)
Δ	perturbation
IEC	International Electrotechnical Commission
MSL	mean sea level
NGI	Norwegian Geotechnical Institute
NREL	National Renewable Energy Laboratory
OWT	offshore wind turbine
LPM	lumped parameter model

According to an engineering note issued by Germanischer Lloyd [8], soil damping is the contributor to OWT damping that is most uncertain. The International Electrotechnical Commission states that "Compared with the other components of the total damping discussed, the characterization and modeling of soil damping is the most complex parameter and has a high damping contribution. Soil damping is a diffuse subject and the contribution to energy dissipation here from is not intuitive in all forms [9]." Det Norske Veritas [10] requires that realistic assumptions with regard to stiffness and damping be made in the consideration of OWT soil-structure interaction but does not recommend a method to estimate soil damping.

Soil damping comes in two main forms: radiation damping (geometric dissipation of waves from spreading) or hysteretic material (also known as intrinsic) damping. Geometric dissipation is negligible for frequencies less than 1 Hz [6,8,11], and the majority of wind and wave loads have frequencies below 1 Hz (e.g. Refs. [12,13]). While the first and second fore-aft and side-to-side natural frequencies of the National Renewable Energy Laboratory 5 MW Reference Turbine (NREL 5 MW) [15] used in this paper are from 0.3 Hz to 3 Hz, the NREL 5 MW under extreme storm loading is dominated by first mode behavior. Because this first mode is at approximately 0.3 Hz, this paper neglects geometric dissipation and focuses solely on hysteretic material damping from soil. This type of soil damping should be more specifically labeled OWT monopile foundation damping (or generally referred to in this paper as "OWT foundation damping") due to the specific formulation and mechanism of hysteretic material soil damping within the OWT soil-structure foundation system.

Some researchers [3,6,11,14] have examined the signals from instrumented OWTs during emergency shutdown (sometimes referred to as a "rotor-stop test"), ambient excitation, and overspeed stops [7] to estimate OWT natural frequency and damping. Subsequently, OWT foundation damping values from 0.25 to 1.5% have been estimated from the residual damping after aerodynamic, hydrodynamic, structural, and nacelle tuned mass damping have been accounted for in numerical modeling. Previous analytical methods have estimated OWT foundation damping using Rayleigh damping as a function of soil strain [6] or from a hysteresis loop created by loading and unloading p-y curves [11].

A two-dimensional finite element model of the NREL 5 MW is used in this paper, taking into account added hydrodynamic mass for the substructure, Rayleigh structural damping, and foundation damping. Hydrodynamic and aerodynamic damping are not included in the scope of this paper, as the focus is specifically on the contributions of foundation damping. Because total damping for the OWT is typically estimated as a linear combination of independently modeled damping sources (e.g. Refs. [6,7,14]), neglecting aerodynamic and hydrodynamic damping is assumed to not influence estimations of foundation damping. Any added mass due to the mobilization of the soil during pile motion is also neglected.

The primary objective of this study is to determine the influence of OWT foundation damping on dynamic response. Section 2 describes the methodology, Section 3 describes how the foundation stiffness and damping were established, and Section 4 describes the combined model of the OWT structure and foundation. In Section 5, the percent of critical damping for the NREL 5 MW OWT model which can be attributed to foundation damping is quantified via logarithmic decrement method of a free vibration time history and compared to the experimental and numerical results available in literature. Subsequently, in Section 6 stochastic time history analysis corresponding to an extreme sea state and extreme wind conditions is used to determine the significance of OWT foundation damping.

2. Methodology

The methodology introduced in this paper uses four types of model: a structural model of the OWT superstructure (the part of the OWT that extends above the mudline), a lumped parameter model (LPM) that approximates the soil-pile system with a rigid bar supported by springs at its tip below the mudline and a mudline damper, an aero-hydro-elastic model constructed in the software package FAST, and a continuum finite element model of the soil-pile system. Each of these models provides a different degree of fidelity with respect to different aspects of OWT loading and response and coupling these models in the manner described here allows the determination of wind and wave loads, soil-pile interaction, and structural dynamics in a way that is not possible within any one of the models or attendant software packages.

The flow chart in Fig. 1 demonstrates the methodology used for determining the linear properties of the LPM which was used to idealize distributed stiffness and damping from the OWT monopile as concentrated stiffness and damping, specifically, a coupled rotational and translational spring and a rotational dashpot. Because soil-pile stiffness and damping are load level-dependent, it was important to ensure that the load level for which the linearized LPM properties were determined was comparable to the load level which the monopile would experience during time history analysis. Several different programs were used in this study and are described in further detail later; the purpose of this section is to demonstrate the interplay of the programs and how they were used to model the OWT support structure.

The primary model of the OWT structure and foundation used for free vibration and stochastic time history analyses was created in the finite element modeling package ADINA [16]. The linearized LPM values, which define the stiffness and damping magnitudes at the mudline of the ADINA model, were iteratively determined as a function of ADINA mudline pile loads using an in-house finite element program created by the Norwegian Geotechnical Institute (NGI) called INFIDEL (INFInite Domain ELement), which models pile-soil interaction without the OWT superstructure [17,18]. In summary, it was necessary to iterate the linearization process until the input quasi-static loads for determining LPM properties in INFIDEL agreed with the output mudline cyclic load amplitude (horizontal mudline force H_x and mudline moment M_ϕ) from the time history analysis in ADINA within 5%. Iteration was required because changes in mudline stiffness conditions for the OWT caused changes in the mudline design loads, which supports the conclusions of other researchers regarding the influence of foundation modeling on mudline loads [19,20].

This methodology (Fig. 1) remains consistent for both the free vibration and stochastic time history analyses, with the exception of load type: for the stochastic time history analyses, the load histories due to wind and wave were generated using NREL's aeroelastic wind turbine simulation program FAST [21] and applied to the ADINA model, whereas free vibration was induced by a tower top displacement directly in ADINA.

The stochastic load time histories generated by FAST were based on a similar structural model as the ADINA model but with a perfectly fixed boundary at the mudline (i.e., no rotation or displacement or damping due to the foundation) and a rigid tower structure. In this way, the loads applied to the ADINA model consist only of external forces and moments induced by wind and waves on the structure. For design purposes, a second iteration would be required where the mudline stiffness and damping conditions are updated in FAST and new loads would be generated until the loads from FAST, ADINA and INFIDEL converge; however, iteration of the stochastic load input was neglected in this study.

3. Foundation stiffness and damping procedures

First we give a basic background for different relevant damping formulations, then the INFIDEL software is described, followed by the procedures for defining springs and dashpots representing the foundation stiffness and damping.

3.1. Damping formulations

As background for the following parts of the paper, this section gives a description of three different damping formulations: (1) hysteretic loss, which is used in the foundation (INFIDEL) model; (2) viscous damping, which is used in the LPM representation of foundation damping in the structural model (ADINA) model; and (3) Rayleigh viscous damping which is used in the structural (ADINA and FAST) models.

Damping mechanisms for mechanical systems may exhibit different mathematical formulations. According to the dynamic correspondence principle we may interpret the loss factor η as the imaginary part of a complex modulus, as here exemplified for the shear modulus G' i.e.

$$G' = G(1 + i\eta) \tag{1}$$

Here, G is the secant shear modulus of the soil. Formally, the loss factor is proportional to the ratio of the energy dissipation per cycle, E_h, divided by the maximum potential energy, E_p, in the same cycle.

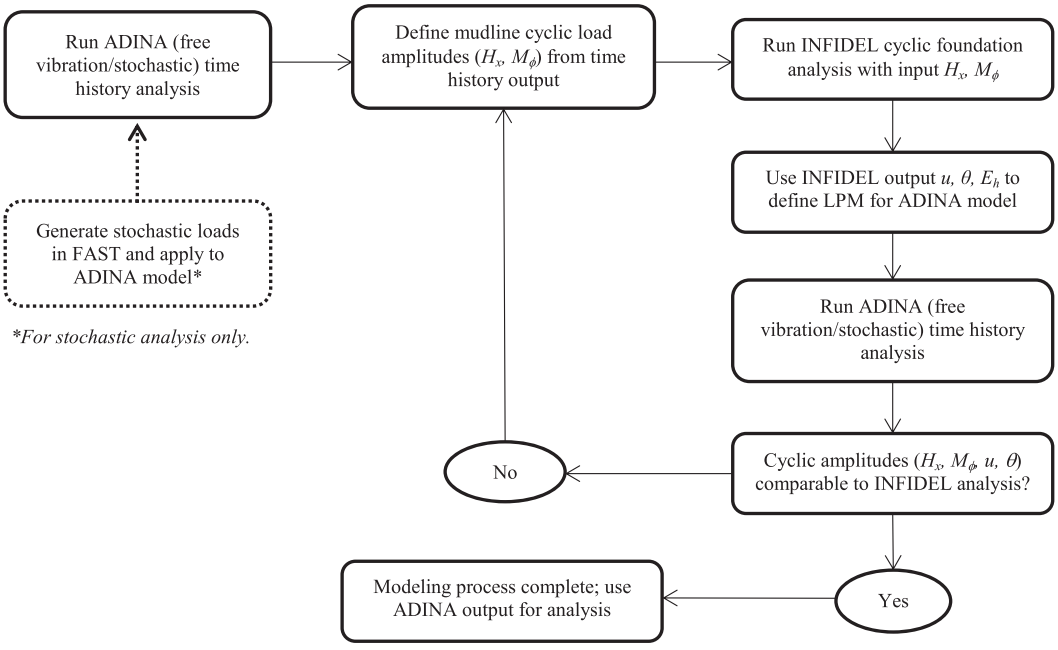

Fig. 1. Flow chart illustrating the iterative methodology for modeling an OWT and foundation including a LPM representing the stiffness and damping of the foundation.

In the case of hysteretic damping, η may be related to a hysteretic damping factor D or quality factor Q through the expression

$$\eta = 2D = \frac{1}{Q} = \frac{1}{2\pi}\frac{E_h}{E_p} \tag{2}$$

A sketch showing the interpretation of the energy loss and potential energy in a stress-strain loop is depicted in the right panel of Fig. 2. The energy loss E_h is interpreted as the area inside the load displacement loop, whereas the potential energy E_p is the area under the triangle.

For a linear single degree of freedom system with a viscous damper (Fig. 2) subject to a harmonic load, the loss factor relates to the viscous damping constant c at a given angular frequency $\omega = 2\pi f$ (where f is the frequency) for a spring-dashpot system according to:

$$\eta = \frac{c\omega}{G} \tag{3}$$

Next, we denote the undamped natural frequency ω_n, the critical viscous damping constant c_{cr} and the fraction of critical viscous damping ξ as:

$$\omega_n = \sqrt{\frac{k}{m}}, c_{cr} = 2\sqrt{k\cdot m}, \xi = \frac{c}{c_{cr}} \tag{4}$$

It can be shown that the loss factor equals twice the degree of critical damping at the natural frequency, i.e.

$$\eta = 2\left(\frac{\omega}{\omega_n}\right)\xi \tag{5}$$

In modeling dynamic systems, damping coefficients are often idealized as constants. Hence, using a frequency independent viscous damping constant c implies a loss factor that increases linearly with frequency. As will be discussed later, the damping parameters (η or c) generally also depend on the load. Furthermore, the concept of Rayleigh damping is frequently encountered in dynamic structural analysis, and represents yet another damping formulation where the damping varies with frequency. For the structural damping in this paper, the fraction of structural critical damping is

$$\xi_{struc} = \frac{\alpha}{2\omega_{n,i}} + \frac{\beta\omega_{n,i}}{2} \tag{6}$$

where ω_n is the ith natural frequency in rad/s, α is a mass-proportional damping coefficient and β is a stiffness-proportional coefficient [22]. All of the different damping formulations above (hysteretic loss, viscous damping, or Rayleigh damping) are present in one or more of the different models which enter the flow chart in Fig. 1.

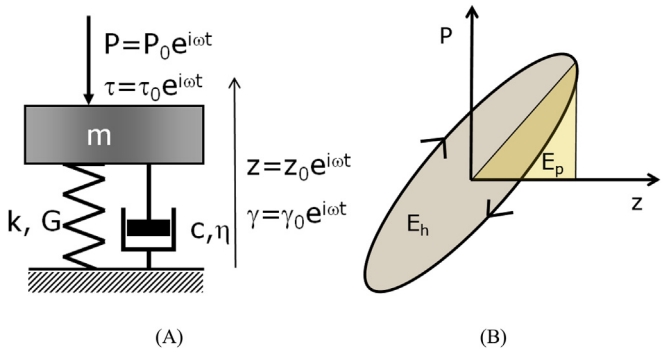

Fig. 2. (A) Sketch of a single degree of freedom spring-dashpot system subject to periodic loading (both force and stress); (B) Sketch showing the interpretation of potential energy and energy loss in a hysteretic loop.

As the soil is assumed to have a hysteretic behavior, below we compute a hysteric foundation-energy loss with the INFIDEL model. This hysteric foundation energy loss is converted to a viscous damping constant in the LPM at the mudline of the ADINA structural model. Furthermore, the structural damping in both the ADINA and FAST structural models is formulated using Rayleigh damping. Therefore, it is important to retain the frequency dependency between the different damping formulations while linking them, particularly if the load frequency spectrum we consider has a large bandwidth.

3.2. Foundation response software

The INFIDEL software is used to compute foundation stiffness and damping which define the LPM at the mudline of the ADINA model. INFIDEL handles axisymmetric three-dimensional quasi-static soil-structure interaction problems with infinite extent and non-linear materials. Circular or elliptic structures are described by Fourier series expansion in the tangential direction. The cyclic loads on the foundation are applied incrementally to compute cyclic displacement and rotation amplitudes of the foundation.

The monopile is modeled as linear elastic, whereas the material model used for the soil is modeled with an isotropic non-linear elastic constitutive model appropriate for undrained materials such as clay. The input parameters for the soil model are the secant shear modulus at small strains, G_0, undrained shear strength, s_u, and Poisson's ratio, ν. The shape of the soil stress strain curve is modeled with the following equation

$$\log\left(\frac{G_t}{s_u}\right) = \log\left(\frac{G_0}{s_u}\right) - C_1\log\left(\frac{\tau_{cy}}{s_u}\right) - C_2\log\left(\frac{\tau_{cy}}{s_u}\right)^2 - C_3\log\left(\frac{\tau_{cy}}{s_u}\right)^3 \tag{7}$$

Where G_t is the tangential shear modulus and τ_{cy} the cyclic shear stress. The three fitting constants, C_1–C_3, control the shape of the stress strain curve and are determined from a so-called modulus reduction curve giving the ratio of the secant shear modulus to the small strain shear modulus for different cyclic shear strain amplitudes as shown in Fig. 3(A). For computation of foundation damping the hysteretic material damping factor, D, as a function of shear strain is also needed as shown in Fig. 3(B). The shapes of the modulus reduction and damping curves are dependent on the plasticity index, and to a lesser degree on the confining pressure and over consolidation ratio (OCR). Further description of modulus reduction and damping curves and how they are determined in laboratory tests are given in e.g. Ref. [23].

For each load amplitude and corresponding shear strain level in the soil, the hysteretic energy density corresponding to one load cycle (area of hysteresis loop) is computed in each element as

$$E_h = 4\pi E_p D \tag{8}$$

and summed over the entire soil volume to compute a corresponding global foundation damping factor,

$$D = \frac{\Sigma E_h}{4\pi\Sigma E_p} \tag{9}$$

where E_h, is the total hysteretic energy for all elements, E_p is the total elastic strain energy for all elements.

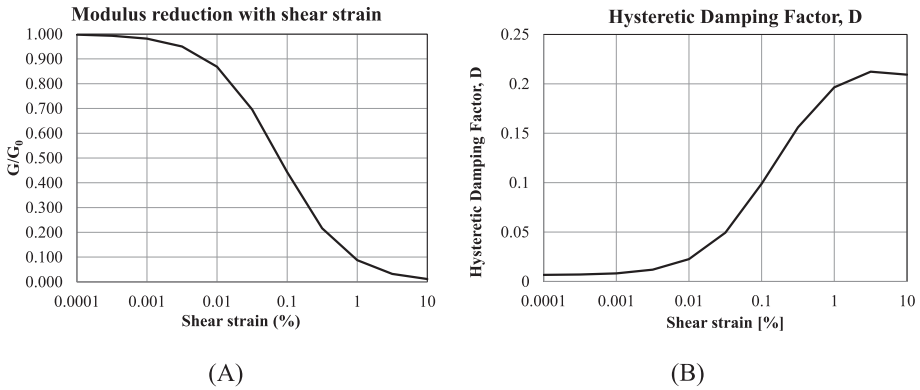

Fig. 3. Examples of (A) the Modulus Reduction curve and (B) the Damping Curve for a representative offshore soil.

3.3. Foundation spring stiffness

Because time history analysis can be computationally demanding, it was desirous to use a linear LPM to represent the OWT monopile foundation stiffness and damping. In an aeroelastic program such as FAST, it is typical to model foundation stiffness as a linear 6 × 6 stiffness matrix at the mudline; however, it is not often possible to define a stiffness matrix at a point in a finite element program such as ADINA. For this paper, out-of-plane (i.e. side-to-side), vertical, and torsional motions of the OWT were not considered, reducing the mudline stiffness matrix to a 2 × 2 mudline stiffness matrix

$$k_{mud} = \begin{bmatrix} k_{xx} & k_{x\phi} \\ k_{\phi x} & k_{\phi\phi} \end{bmatrix} \tag{10}$$

in which the subscript x refers to horizontal in-plane translation degree of freedom and the ϕ refers to the in-plane rotational degree of freedom. In order to simplify the model by decoupling the stiffness matrix, the off-diagonal coupled stiffness coefficients ($k_{x\phi}$ and $k_{\phi x}$) were kinematically condensed into decoupled horizontal translation (k_{xx}') and rotation ($k_{\phi\phi}'$) springs located at the end of a rigid bar of length L_{eq} (Fig. 5). The LPM properties k_{xx}', $k_{\phi\phi}'$, and L_{eq} were determined using NGI's in-house finite element program INFIDEL.

For a linear elastic stiffness matrix the rigid bar length is

$$L_{eq} = \frac{k_{x\phi}}{k_{xx}}. \tag{11}$$

For a nonlinear foundation behavior, the length L_{eq} can be found with the help of two INFIDEL analyses using the same horizontal load but slightly different moments. For a small difference in moment the difference in translation at the mudline will be due to a rotation around a point at distance, L_{eq}, below the mudline. Using the perturbation in the moment, ΔM_ϕ, L_{eq} is determined by

$$L_{eq} = -\frac{u(H_x, M_\phi) - u(H_x, M_\phi + \Delta M_\phi)}{\theta(H_x, M_\phi) - \theta(H_x, M_\phi + \Delta M_\phi)}. \tag{12}$$

Subsequently, the decoupled spring stiffnesses k_{xx}' and $k_{\phi\phi}'$ can then be calculated as

$$k_{xx}' = k_{xx} = \frac{H_x}{u + L_{eq}\theta} \tag{13}$$

and

$$k_{\phi\phi}' = \frac{M_\phi - L_{eq}H_x}{\theta} \tag{14}$$

3.4. Foundation viscous dashpot

Because the LPM condenses soil-pile interaction, a viscous rotational dashpot was introduced at the mudline to represent concentrated hysteretic damping from cyclic pile-soil interaction. Research has shown that pile head rotation controls mudline serviceability limit states for OWT monopiles [24] and moment typically dominates mudline loading for OWT monopiles, thus the authors believe that a rotational dashpot may more appropriately represent foundation damping than a traditional horizontal translation dashpot. While using both a rotational and translational dashpot is possible, it is not clear that one could decompose the hysteretic energy dissipation in the INFIDEL analysis into parts corresponding to translation and rotation degrees of freedom. Therefore, since a unique solution would not be possible for the parameters of the translational and rotational dashpots, computation of those parameters would depend on some *ad hoc* assumption regarding the partitioning of damping to the rotation and translation degrees of freedom. Consequently, all foundation damping here has been assigned to the rotational degree of freedom.

The computed hysteretic energy loss (E_h) dissipated from a single load cycle in INFIDEL can be converted into a viscous rotation damper. For a harmonic rotation at the mudline to have the same energy loss in the dashpot in one cycle as hysteretic energy loss in the foundation, the dashpot viscous damping constant is computed as

$$c_{\phi\phi} = \frac{E_h}{2\theta^2\pi^2 f} \tag{15}$$

Where θ is the rotation amplitude in radians, and f is the loading frequency, which can be estimated from the Fourier spectrum of the loads. The resulting foundation dashpot coefficient is therefore dependent on 1) the load level (since hysteretic energy, E_h, varies with load level), 2) the cyclic rotation amplitude and 3) the loading frequency. A few iterations between the structural dynamic analysis and foundation analysis may be needed to determine an appropriate dashpot value for a specific load level, rotation amplitude and loading frequency; Fig. 1 outlines the iterative methodology.

Because the mudline load conditions during free vibration differ from the stochastic time history analysis presented below, different

LPMs were developed to more appropriately match the mudline conditions for each type of analysis.

4. Combined OWT and foundation model

The NREL 5 MW Reference Turbine (Table 1) is used in this paper to quantify the significance of foundation damping for monopile-supported OWTs. A two-dimensional finite element model of the NREL 5 MW was created in ADINA, supported by a LPM representing a 34 m-monopile in clay for a site with an assumed mean sea level (MSL) of 20 m and a hub height of 90 m (Fig. 5).

The finite element model of the NREL 5 MW was defined by elastic Euler-Bernoulli beam elements with linear elastic material properties. The modulus of elasticity for the tower and substructure was assumed to be 210 GPa with a density of 8500 kg/m^3 to account for the additional mass of paint, flanges, bolts, etc. [15]. The OWT model used a lumped mass matrix, with a concentrated mass of 350,000 kg assigned to the top of the finite element model to take into account the mass of the blades and rotor-nacelle assembly. The blades themselves were not modeled because it was assumed that aside from the mass added to the tower top, parked and feathered blades have minimal impact on the natural frequency and damping of the OWT.

The wall thickness for the OWT was increased from the values found in Ref. [15] in order to increase the stiffness of the support structure to maintain a natural frequency of approximately 0.3 Hz. Maintaining this natural frequency ensured that the dynamic loading from the FAST model (which was fully fixed at the mudline) was consistent with the dynamic behavior exhibited by the ADINA model (with flexible mudline due to the LPM). A comparison of the ADINA and FAST tower modes and frequencies was performed in order to ensure a consistent dynamic model. The resulting height distribution of the moment of inertia of the OWT is compared with original NREL model in Fig. 4.

Added hydrodynamic mass was incorporated in the OWT substructure to represent hydrodynamic interaction effects using the simplified method for cylindrical towers proposed by Ref. [25]. Added hydrodynamic mass was calculated for each substructure element, divided by cross-sectional area, and included in the unique definition of material density per substructure element.

Structural Rayleigh damping of 1.00% was assumed for the NREL 5 MW, which is consistent with the definition of the structure in Ref. [15]. Structural damping was applied to the tower and substructure of the ADINA finite element model using Rayleigh damping.

Assuming that source of damping can be modeled separately and superimposed (per [6–8,14]), hydrodynamic and aerodynamic damping were neglected to more precisely focus on the significance of OWT foundation damping.

Table 1
Offshore wind turbine model properties.

Property	NREL 5 MW
Rating	5 MW
Hub height	90 m
Rotor diameter	126 m
Tower base, tower top diameter	6.0 m, 3.9 m
Nacelle & rotor mass	350,000 kg
Tower MASS	347,000 kg
Mean sea level	20 m
Substructure diameter, wall thickness	6.0 m, 0.11 m
Pile diameter, wall thickness	6.0 m, 0.09 m
Pile embedment depth	34 m

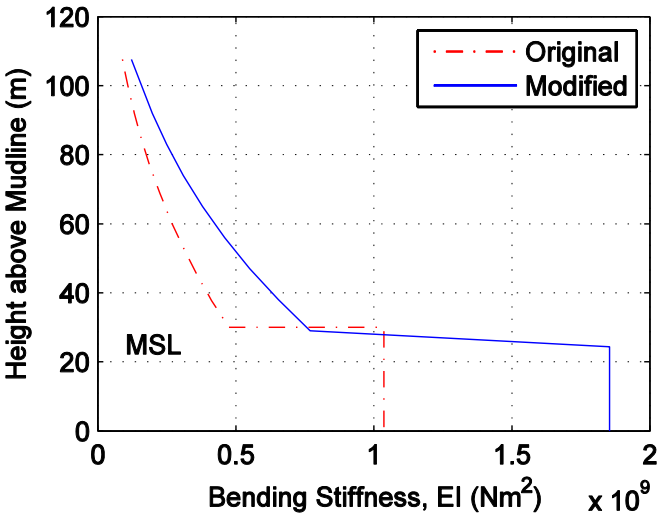

Fig. 4. Moment of inertia over support structure height for original vs. modified NREL 5 MW reference turbine.

4.1. Soil and foundation properties

The soil profile considered in this paper was divided into three layers (soft clay, stiff clay, and hard clay) to account for changes in soil parameters with depth (Fig. 6). Input parameters were based on a specific North Sea offshore site as shown in Fig. 6. Based on the established soil profile and a loading frequency of 0.3 Hz, curves for shear modulus reduction and damping versus shear strain were established based on equations given in Ref. [23] assuming a density of 2000 kg/m^3, over consolidation ratio of 10, and plasticity index of 20 for all layers. In principal, different modulus reduction and damping curves should be used for each layer since modulus reduction depends on confining stress and depth below the mudline. Since the effect of confinement on the modulus and confinement curves is small compared the changes in the shear modulus and shear strength themselves, the same modulus and damping reduction curves have been used for all three layers (Fig. 3). The resulting stress strain curves for the three layers are shown in Fig. 7.

When computing the foundation stiffness and damping with INFIDEL, the monopile was assumed to be in full contact with the soil, i.e. effects of gapping due to non-linear compression of the soil on the side of the pile and/or erosion have not been considered. Since gapping would result in a nonlinear and potentially asymmetric foundation stiffness, it could not be modeled using the current approach; however, the mudline displacements identified in this study (approximately 0.01 m) are unlikely to produce a gapping effect. Furthermore the mudline loads (i.e. the horizontal force, H_x and moment, M_ϕ) are assumed to be in phase and were increased proportionally. Fig. 8 gives an example of INFIDEL results showing the distribution of the ratio between cyclic shear stress and shear strength. The soil in the vicinity of the upper part of the monopile is the most strained and provides the largest contribution to the overall foundation damping.

5. Free vibration analysis

A free vibration analysis was conducted on the NREL 5 MW finite element model in ADINA to quantify the contribution of foundation damping to global damping. The free vibration analysis was performed by gradually displacing the tower top by 0.1 m, holding the displacement for 10 s to reduce transient vibrations, and then releasing the applied displacement to allow the OWT to vibrate

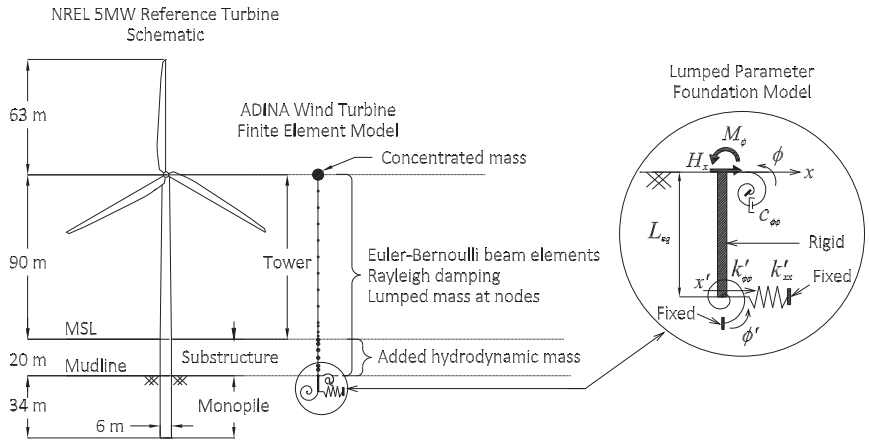

Fig. 5. Offshore wind turbine models.

freely, see Fig. 9. The 0.1 m displacement was selected to fall in the middle of the range of tower top displacements found to occur during the stochastic time history analysis. Imposing a larger displacement would result in smaller foundation stiffness and larger foundation damping.

Global damping was then quantified from the free vibration time history using the logarithmic decrement method, where the logarithmic decrement

$$\delta = \frac{1}{n}\ln\left(\frac{A_1}{A_n}\right) \tag{16}$$

in which A_1 and A_n are two successive amplitudes n periods apart. A log fit of successive amplitudes was fit to the response to estimate δ. The global damping ratio ξ can then be calculated as a function of δ by

$$\xi = \frac{1}{\sqrt{1+(2\pi/\delta)^2}} \tag{17}$$

which here estimates the global damping associated with the first structural mode of the OWT.

Rayleigh structural damping was applied to the OWT superstructure and not the LPM, because the concentrated rotational dashpot was considered to account for all foundation-related damping. Because Rayleigh damping is a function of natural frequency which is in turn a function of the finite element stiffness matrix, neglecting to apply Rayleigh damping to the LPM resulted in an inaccurate calculation of ξ_{struc} according to Eq. (6). In order to achieve $\xi_{struc} = 1.00\%$, the Rayleigh damping mass coefficient α was held constant while stiffness coefficient β was increased such that the damping obtained from the logarithmic decrement of free

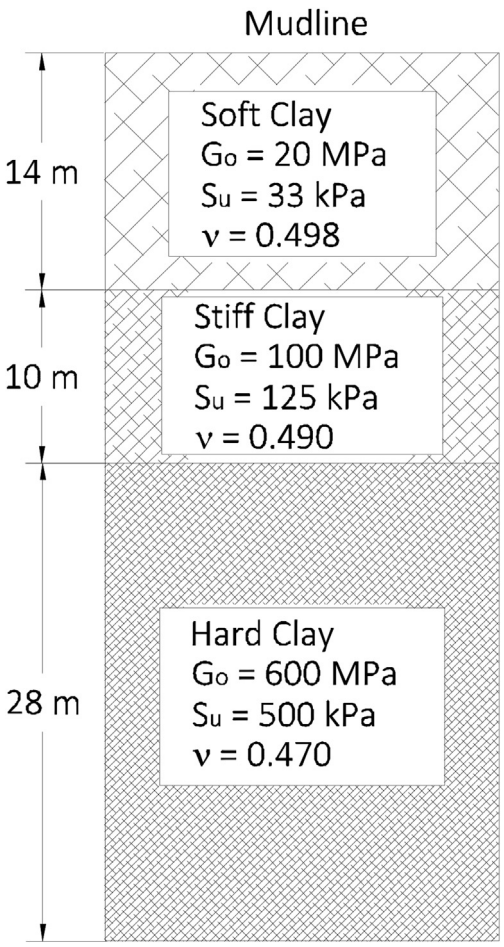

Fig. 6. Representative North Sea offshore soil profile used for estimating contributions of foundation damping via INFIDEL.

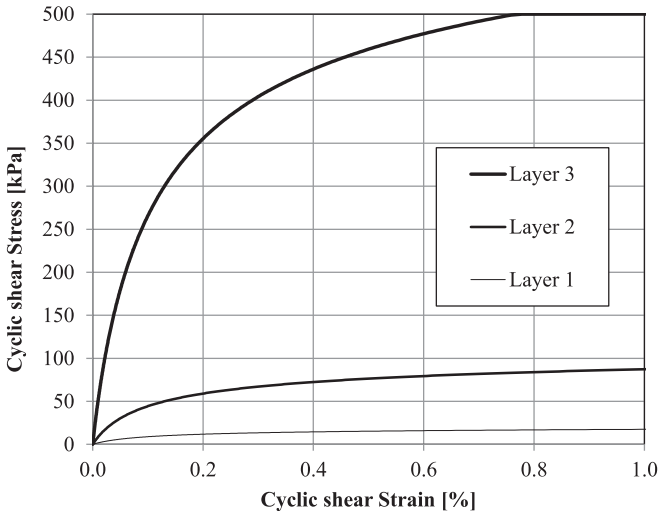

Fig. 7. Shear stress versus shear strain for the three different soil layers.

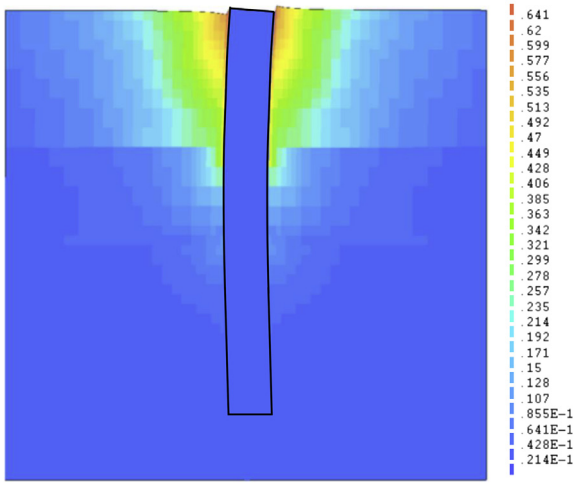

Fig. 8. Distribution of shear stress mobilization , i.e. ratio between maximum shear stress and shear strength.

vibration was equal to 1.00%, with the mudline dashpot $c_{\phi\phi} = 0$ and $\omega_{n1} = 2\pi f$ per Table 3 (as load frequency is equal to natural frequency in the case of free vibration). While this method of Rayleigh damping is only applicable to the first mode of vibration, it is assumed that first mode behavior is dominant for the NREL 5 MW turbine.

It is arguable what the appropriate mudline load level is best for assessing linear stiffness and damping for the LPM under free vibration time history analysis (e.g. the maximum, average, or root-mean-square mudline load amplitudes could be used to assess LPM properties). While the maximum mudline load would lead to the lowest mudline stiffness due to non-linear soil-pile resistance, it would also lead to a higher levels of strain in the soil and consequently the highest amount of damping [23]. To demonstrate the importance of mudline loading on LPM properties, a free vibration case was considered by displacing the OWT tower top by 0.1 m. LPM properties were calculated based on the static mudline loads induced by tower top displacement, u_{top}.

Iteration was required to achieve agreement between the mudline loads specified in the INFIDEL cyclic foundation analysis and the output static displacement load from ADINA as described the methodology section and Fig. 1. A comparison of the INFIDEL input and ADINA output demonstrates good agreement in load amplitudes and response (see Table 2).

Table 2
Comparison of the peak mudline conditions used in INFIDEL cyclic soil-pile analysis and ADINA free vibration time history analysis for 0.1 m Tower top displacement.

Parameter	INFIDEL analysis	Free vibration in ADINA
Shear, H_x	158 kN	156 kN
Moment, M_ϕ	−16.0 MNm	−15.9 MNm
Displacement, u	1.19×10^{-3} m	1.28×10^{-3} m
Rotation, θ	-1.52×10^{-4} rad	-1.62×10^{-4} rad
Load frequency, f	–	0.307 Hz
Hysteretic energy loss, E_h	0.130 kJ	–
Foundation damping factor, D	0.79%	–
Structural damping ratio, ξ_{struc}	–	1.00%
Foundation damping ratio, ξ_{fdn}	–	0.17%

Table 3
Lumped parameter foundation model properties for ADINA free vibration analysis for 0.1 m Tower top displacement.

Lumped parameter model property	$u_{top} = 0.1$ m
L_{eq}	7.60 m
k_{xx}'	3.89×10^{9} N/m
$k_{\phi\phi}'$	1.14×10^{11} Nm/rad
$c_{\phi\phi}$	9.34×10^{8} Nm-s/rad

The results in Table 2 were used as input to Eqs. 11–14 in order to obtain the LPM properties in Table 3.

An example of the 0.1 m free vibration time history from ADINA for the NREL 5 MW finite element model is shown in Fig. 10.

It can be visually concluded from Fig. 10 that the inclusion of mudline foundation damping effects tower top vibration, with the damped mudline vibration amplitude decreasing slightly faster than the case considering only structural damping. From the logarithmic decrement method, the damping ratio from the $u_{top} = 0.1$ case was $\xi_{tot} = 1.17\%$ − subtracting the 1.00% Rayleigh structural damping (ξ_{struc}), this means that 0.17% of damping can be attributed to foundation damping (ξ_{fdn}). The LPM calculations and resulting ξ_{struc} are sensitive to input load level; if the free vibration analysis is repeated for a tower top displacement of $u_{top} = 0.16$ m for instance, ξ_{struc} increases to 0.28%.

Table 4 compares the results of the free vibration study and of other foundation damping studies for OWTs. The results of the current analysis yield a relatively low amount of foundation damping compared to the damping found by other researchers, but

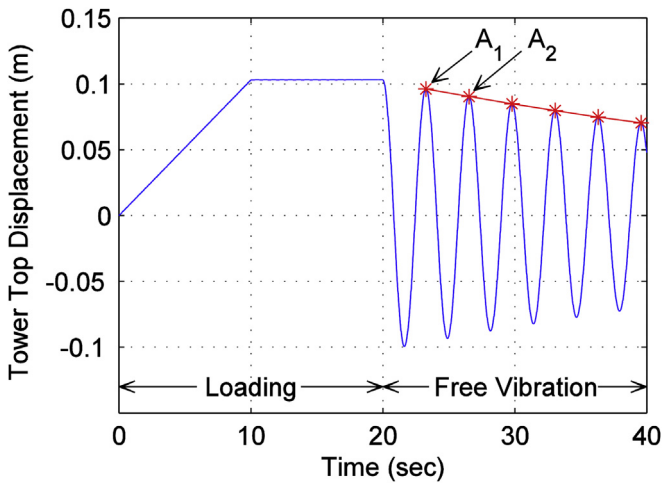

Fig. 9. Free vibration analysis time history.

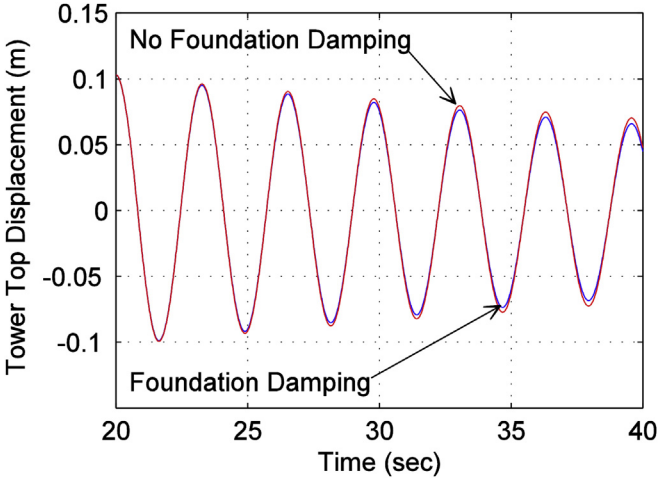

Fig. 10. Free vibration of the NREL 5 MW reference turbine, with and without foundation damping.

Table 4
Summary of monopile-supported offshore wind turbine damping results from literature.

	Tarp-Johansen *et al.* (2009)	Versteijlen *et al.* (2011)	Damgaard *et al.* (2012)	Damgaard *et al.* (2013)	Shirzadeh *et al.* (2013)	Carswell *et al.* (2014)
Method	Experimental	Experimental	Experimental	Experimental	Experimental	Numerical
Analysis	3D FEM	Modified *p-y*	Hysteretic *p-y*	Hysteretic *p-y*	HAWC2, Rayleigh	3D and 2D FEM
Turbine	3.5 MW (Scaled NREL 5 MW)	Siemens 3.6 MW	–	Vestas V90-3 MW	Vestas V90-3 MW (Scaled NREL 5 MW)	NREL 5 MW
Soil profile	Generalized sandy or clayey North Sea	–	Top layer loose sand, very stiff to very hard clay	Medium dense sand and soft clay	Dense sand with layer of stiff clay	Soft, stiff, and hard clay
ξ_{fdn}	0.56%–0.80%	1.5%	0.58%	0.8–1.3%	0.25%	0.17%–0.28%
ξ_{struc}	0.19%	1.5%	0.19%	–	0.6%	1.00%
Sum:	0.75–0.99%	3.0%	0.77%	0.8–1.3%	0.85%	1.17%–1.28%

are similar to the experimental results estimated by Shirzadeh *et al.* (2011) [7], Damgaard *et al.* (2012) [14] and to the minimum of the range defined by Tarp-Johansen *et al.* (2009) [6]. The majority of the researchers provide free vibration response of the OWT in terms of acceleration; however, in the case of [3], the loads at the bottom of the tower would indicate rough agreement with the mudline loads analyzed in this paper.

Several different methods were used to estimate foundation damping, so it is unsurprising that a variation in results was observed. Damgaard *et al.* (2012) and (2013) [8,11] used a hysteretic *p-y* method, wherein a hysteretic loop was defined using a traditional *p-y* spring-supported pile per [10], whereas Versteijlen *et al.* (2011) [3] used modified *p-y* curves adjusted for rigid-behavior monopiles with damping proportional to spring stiffness. Minimal description of the soil modeling was given in Shirzadeh *et al.* (2013) [7], only that a form of Rayleigh damping was used to apply damping as part of the input for the aeroelastic code HAWC2. Most similarly to the process used in this paper, Tarp-Johansen *et al.* (2009) [6] estimated foundation damping from a three dimensional solid finite element model of the soil and OWT support structure, assuming generalized linear elastic soil material properties. Soil damping was taken into account as a form of Rayleigh damping, assuming a loss factor of 10%.

Germanischer Lloyd [8] experimentally determined a foundation damping value of 0.53%, theoretically calculated foundation damping of 0.88%, but also lists estimations from 0.6% to 1% depending on soil behavior assumptions. It can be concluded therefore that a certain amount of variation in OWT foundation damping should be expected, and that these results are sensitive to modeling assumptions.

6. Stochastic time history analysis

6.1. Load input

The finite element model of the NREL 5 MW Reference Turbine was subjected to six different 1-hr stochastic load histories corresponding to extreme wave and wind loading to determine the effects of OWT foundation damping on the OWT response.

NREL's aeroelastic code FAST [21] was used to generate stochastic time history loads due to wind and waves. FAST models wind turbines as a system of rigid and flexible bodies and computes wind turbine response to stochastic loading using lumped parameter and modal analysis [26]. The OWT loads were calculated per IEC design load case 6.1a [9] using the environmental site conditions shown in Table 5.

Table 5
Environmental site conditions.

50-year conditions	Value
Water depth	20 m
10-min average hub height wind speed	34 m/s
Significant wave height	8.5 m
Peak spectral wave period	10.3 s

IEC dictates that for design load case 6.1a, six 1-hr simulations for different combinations of extreme wind speed and extreme sea state must be performed considering misalignment and multi-directionality. This study considers six 1-hr load time histories with co- and uni-directional wind and waves, which is conservative from a design perspective; however, it is assumed that co- and uni-directional loading will best demonstrate the effects of OWT foundation damping in a two-dimensional, parked wind turbine context.

Wind loading was applied to the NREL 5 MW finite element model in ADINA via tower top force and moment histories generated in FAST, and wind loads on the tower were neglected (Fig. 11). Tower wind loads are not directly calculated by FAST (version 7, available during the conduct of this study), and were thus excluded from all of the modeling included here to preserve consistency with FAST. If tower wind loads were included in the analysis mudline moment and shear would increase, the stiffness of the foundation would decrease and the amount of foundation damping would increase. Wind speed is assumed to increase with height according to a power law, causing a net negative moment (according to a right-hand rule sign convention, per Fig. 11) around the nacelle due to wind on the parked and feathered rotors due to their configuration with a single blade pointed upward.

Wave kinematics were generated in FAST at seven nodes along the OWT structure. Wave forces per unit length were calculated

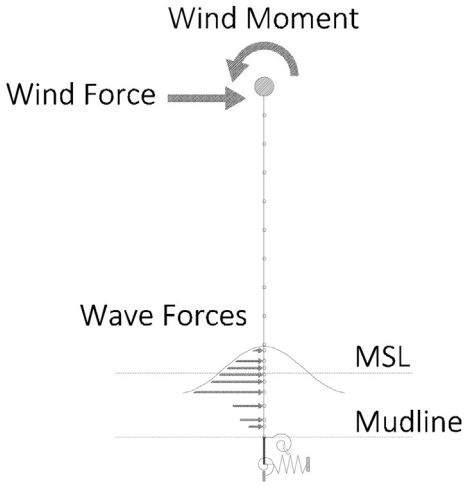

Fig. 11. Example time step of wave force loading on ADINA NREL 5 MW finite element model.

from the wave kinematics using Morison's equation for a cylinder multiplied by a tributary length to approximate the wave shear profile (Fig. 11). A fluid density of 1027 kg/m^3 was assumed for seawater and C_m and C_D were taken to be 1.75 and 1.26 respectively for a substructure with intermediate surface roughness.

Because the viscous mudline dashpot $c_{\phi\phi}$ was derived for a single degree of freedom system subjected to harmonic loading and because the actual loading of an OWT is stochastic, it was necessary to establish a harmonic load amplitude that was in some sense representative of the load amplitudes experienced during the stochastic loading. The load amplitude level selected was three standard deviations (3σ, Fig. 12) from the mean of the stochastic loading history. This load amplitude appeared to best represent the amplitude of the stochastic loading – the 3σ limit is only exceeded by the most severe load cycles – and had little variation across the six 1-hr stochastic time histories. Due to the iteration required, only one of the 1-hr stochastic time history was used for determining LPM properties for the six simulations (Fig. 12).

Several iterations were required to obtain mudline load and rotation amplitudes which agreed with those used in cyclic foundation analysis. Table 6 compares the load and response amplitudes of the single stochastic time history to those from the cyclic foundation analysis. The resulting LPM properties are given in Table 7.

Logarithmic decrement of the OWT model supported by the LPM properties in Table 7 yielded ξ_{fdn} of 0.72%, which is significantly larger than the results from the 0.1 m free vibration analysis (0.17%). The higher damping is due primarily to the increase in E_h associated with the higher load levels (−41.2 MNm for the 3σ stochastic results vs. −16.0 MNm for the 0.1 m free vibration analysis).

6.2. Stochastic time history results

Six different 1-hr stochastic load histories were analyzed for the NREL 5 MW for two cases: (1) Rayleigh structural damping alone ("No Foundation Damping") and (2) Rayleigh structural damping in addition to mudline OWT foundation damping ("Foundation Damping") for a total of 12 stochastic time histories. The reduction in mudline moment amplitude attributed to foundation damping can be seen in the example time history shown in Fig. 13.

A summary of the maximum and standard deviation of mudline load and displacement amplitudes as well as maximum tower top amplitude u_{top} from each time history can be seen in Table 8.

While mudline moment and shear were highly correlated (the average correlation coefficient was approximately 0.8), mudline moment was more significantly reduced by foundation damping than mudline shear (Table 9). A decrease in wind or wave force is magnified by the length of the moment arm to the mudline; consequently, a small decrease in OWT support structure forces results in a non-proportional decrease at the mudline. Notably, both maximum mudline moments as well as the 3σ estimation of cyclic moment amplitude decreased by an average of 7–9% due to foundation damping; additionally, it can be noted from Table 8 that the standard deviation of mudline moment decreased by nearly 9% with the inclusion of foundation damping.

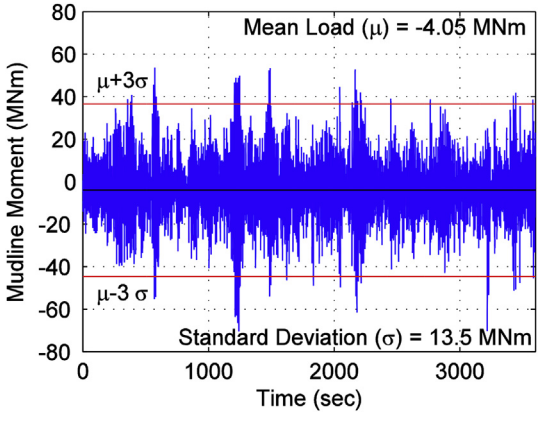

Fig. 12. Time history of mudline moment indicating three standard deviation amplitude.

Table 6
INFIDEL foundation analysis and ADINA stochastic time history analysis results.

Mudline condition	INFIDEL foundation analysis	Damped mudline stochastic time history (3σ)
Shear, H_x	2610 kN	2606 kN
Moment, M_ϕ	−41.2 MNm	−40.5 MNm
Displacement, u	6.45×10^{-3} m	6.73×10^{-3} m
Rotation, θ	-6.23×10^{-4} rad	-6.55×10^{-4} rad
Dominant load frequency, f	–	0.302 Hz
Hysteretic energy loss, E_h	7.61 kJ	–
Foundation damping factor, D	2.88%	–
Structural damping ratio, ξ_{struc}	–	1.00%
Foundation damping ratio, ξ_{fdn}	–	0.72%

Mudline displacement and rotation amplitudes decreased similarly with foundation damping, with an average reduction of 3–4% in the 3σ estimation of cyclic amplitude and 5–6% in the average maximum from the six time histories.

A rainflow count of mudline moment from all six stochastic analyses was performed to further quantify the effect of foundation damping on load cycle amplitudes (Fig. 14). The rainflow counts indicate reductions (note that the vertical axis is a log scale) in cycle counts across the range of cycle amplitudes. This indicates that foundation damping may serve to reduce fatigue damage. This effect requires substantial further study however, since the 50-year storm conditions investigated here do no occur frequently and do not contribute significantly to lifetime fatigue damage. Fatigue damage estimates, therefore, would require simulation of response over a range of operational and non-operation wind speeds amounting to at least many tens of sets of simulations. Such work is the subject of ongoing research on the part of the authors.

For loading frequencies closer to the natural frequency, the juxtaposition of load frequency and natural frequency content would produce a more pronounced reduction in higher amplitude cycles. Fig. 15 depicts the relationship between the Kaimal and JONSWAP power density spectra for wind and waves (respectively) and the ratio of dynamic amplification factors for the cases with ($R_{d,tot}$) and without foundation damping ($R_{d,struc}$) included, where

$$R_d = \frac{1}{\sqrt{\left(1-\omega^2/\omega_n^2\right)^2 + \left(2\xi\omega/\omega_n\right)^2}} \tag{18}$$

in which ω is the loading frequency and ω_n is the natural frequency in rad/s. A free vibration analysis of the NREL 5 MW supported by

Table 7
Lumped parameter foundation model properties for stochastic time history analysis.

Lumped parameter model property	Value
L_{eq}	9.12 m
k_{xx}'	3.38×10^9 N/m
$k_{\phi\phi}'$	1.04×10^{11} Nm/rad
$c_{\phi\phi}$	3.29×10^9 Nm/s

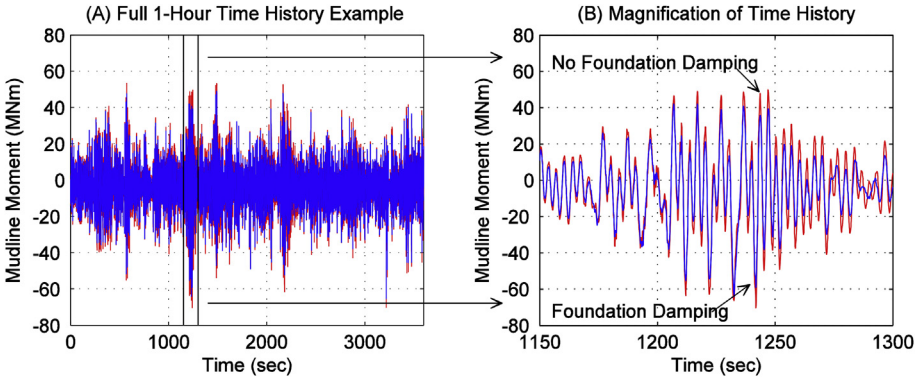

Fig. 13. Example mudline moment time history results.

Table 8
Maximum and standard deviation of mudline reactions.

Case	Time history							Statistics	% Change
	Reaction	1	2	3	4	5	6	Average	
No foundation damping	H_x (kN)	4229	3963	4388	3881	4025	4110	4099	–
	σ (kN)	864	880	861	850	894	896	874	–
	M_ϕ (MNm)	−70.5	−60.5	−74.0	−60.4	−71.5	−77.2	−69.0	–
	σ (MNm)	13.5	13.2	12.9	13.5	13.9	14.1	13.5	–
	u (10^{-3} m)	11.9	9.9	12.5	10.1	11	12.4	11.3	–
	σ (10^{-3} m)	2.24	2.25	2.21	2.23	2.33	2.34	2.27	–
	θ (10^{-4} rad)	−11.6	−9.71	−12.2	−9.87	−10.9	−12.2	−11.1	–
	σ (10^{-4} rad)	2.18	2.18	2.14	2.17	2.26	2.27	2.20	–
	u_{top} (m)	0.322	0.272	0.261	0.321	0.309	0.322	0.301	–
	σ (m)	6.49	6.15	5.97	6.50	6.60	6.72	6.41	–
Foundation damping	H_x (kN)	4232	3863	4213	3769	3962	4009	4008	−2.2
	σ (kN)	864	880	861	850	894	896	874	0
	M_ϕ (MNm)	−65.5	−56.5	−70.8	−55.6	−65.7	−70.0	−64.0	−7.2
	σ (MNm)	12.1	12.1	12.0	12.2	12.8	12.8	12.3	−8.8
	u (10^{-3} m)	11.4	9.52	11.9	9.23	10.9	11.8	10.8	−4.4
	σ (10^{-3} m)	2.15	2.18	2.15	2.14	2.25	2.27	2.19	−3.5
	θ (10^{-4} rad)	−11.0	−9.13	−11.7	−8.97	−10.6	−11.5	−10.5	−5.4
	σ (10^{-4} rad)	2.08	2.10	2.07	2.07	2.17	2.20	2.11	−4.1
	u_{top} (m)	0.258	0.249	0.257	0.291	0.274	0.287	0.269	−10
	σ (10^{-2} m)	5.48	5.34	5.32	5.51	5.73	5.78	5.53	−14

the LPM defined by Table 7 yielded $\xi_{fdn} = 0.72\%$, which broadly agreed with the results presented earlier given the amplitudes of u_{top}, u, and θ. Despite the difference in damping ratio for the two cases considered (1.72% and 1.00% for the cases with and without foundation damping, respectively), the ratio of dynamic amplification factors considering a 0.1 Hz wave load frequency is effectively 1. Given Fig. 15a, it is apparent that the tails of the wind and wave spectra coincide with the dynamically amplified region, and that increased frequency content from higher wave frequency (i.e., lower peak spectral period) would have a significant effect on mudline loading. An examination of Fast Fourier Transforms (Fig. 15b) of the mudline moment for the stochastic time histories with and without foundation damping demonstrated a 40% reduction in the magnitude of the spectral response at the first natural frequency (for which the foundation was calculated). Estimation of OWT natural frequency in a design context is inherently

Table 9
Summary of average and maximum reduction in mudline response from foundation damping, considering time history maxima and three standard deviation estimation of cyclic amplitude.

Mudline response	Cyclic amplitude, 3σ		Maximum response	
	Average reduction	Maximum reduction	Average reduction	Maximum reduction
H_x (kN)	0.48%	0.52%	2.2%	4.0%
M_ϕ (MNm)	8.9%	10%	7.2%	9.3%
u (10^{-3} m)	3.4%	4.0%	4.5%	8.6%
θ (10^{-4} rad)	3.9%	4.7%	5.5%	9.1%

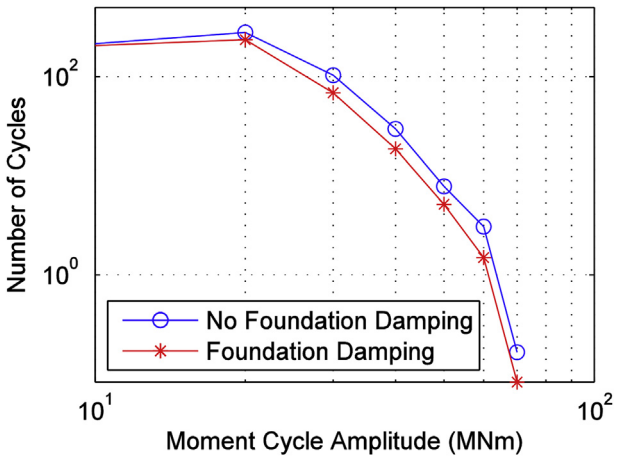

Fig. 14. Average rainflow count results of mudline moment from six stochastic time history simulations.

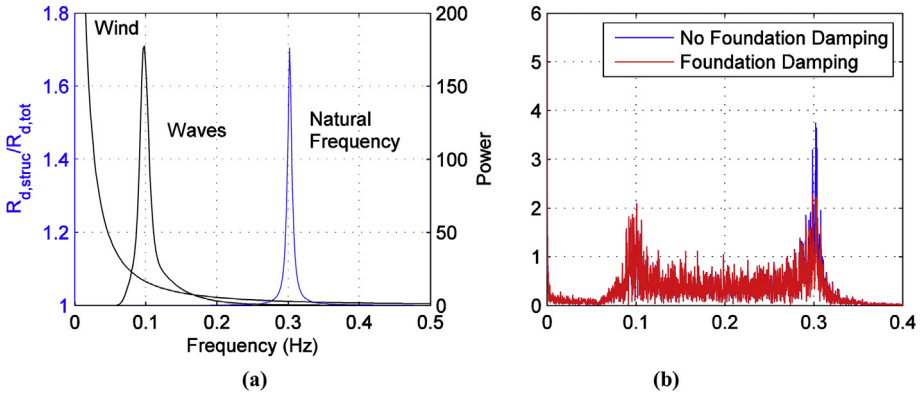

Fig. 15. (a) Ratio of dynamic amplification factors for cases with and without foundation damping compared to load spectra and (b) spectral response with and without foundation damping.

uncertain and dependent on available data and modeling techniques; consequently, the sensitivity of the load amplification is reliant on the accurate estimation of both OWT natural frequency and load frequency spectra.

7. Conclusion

The proximity of wind and wave load frequencies to offshore wind turbine (OWT) natural frequency necessitates a thorough examination of different sources of damping – aerodynamic, hydrodynamic, structural, and soil damping – in order to reduce design loads and improve offshore wind energy economics. Of all the sources of damping, soil damping has been the least studied and presents the largest discrepancy between measured and theoretical results [8]. Because the effect of soil damping on OWT dynamics is innately a function of soil-pile interaction, a more appropriate term for this dynamic quantity is "foundation damping." In an effort to better quantify foundation damping, this paper presents a method for converting hysteretic energy loss into a viscous, rotational mudline dashpot to represent OWT foundation damping for a lumped parameter model (LPM).

A two-dimensional finite element model of the NREL 5 MW Reference Turbine [15] was examined in free vibration and stochastic time history in order to ascertain the significance of OWT foundation damping. Using logarithmic decrement, mudline OWT foundation damping was estimated to contribute 0.17%-0.28% of critical damping to total OWT damping. While these results are at the lower end of the range of results from other researchers [6,7,11,14], they are broadly in agreement with previous estimates of foundation damping, taking into account differences in soil type, monopile foundation, wind turbine, and mudline load conditions.

The mudline response from six 1-hr stochastic time histories was used to assess the significance of OWT foundation damping during extreme loading due to wind and waves. Three standard deviations (3σ) were used as a measure of cyclic amplitude for mudline response (i.e., shear, moment, displacement, and rotation) and to determine the properties of the LPM. Logarithmic decrement of the 3σ LPM (Table 7) yielded 0.72% critical damping from the monopile foundation, which was significantly larger than the free vibration results primarily due to the increase in hysteretic energy. Including OWT foundation damping reduced maximum mudline moment by 7-9%, but had a much less significant effect on mudline shear (approximately 2% reduction). Foundation damping caused an average reduction of approximately 3–5% in both the maximum and 3σ amplitudes of mudline displacement and rotation. The results shown here emphasize the importance of modeling assumptions in foundation damping estimation, with particular attention to the mudline loads used in this paper to determine the properties of the LPM.

Significant reductions in high amplitude cycle counts were observed considering the average rainflow count of mudline moment from the six stochastic time histories. These results are contingent upon the estimation of OWT natural frequency and environmental load conditions, and the effects of foundation damping are expected to be more pronounced in conditions with peak wave frequencies closer to the natural frequency.

Further research is required to determine the impact of foundation damping on OWTs during other design conditions (operation or emergency shutdown, e.g.) as well as the significance of foundation damping in a fatigue limit state.

Further investigation is necessary to understand the influence of the many aspects of soil behavior on the foundation stiffness and damping, e.g. dilative materials, such as dense sand, partially drained materials, scour and gapping that can cause loss of contact between foundation and soil, and combined static and cyclic loading.

Acknowledgments

This research was supported through the NSF-sponsored IGERT: Offshore Wind Energy Engineering, Environmental Science, and Policy (Grant Number 1068864) as well as grants CMMI-1234560 and CMMI-1234656 and the Norwegian Geotechnical Institute.

References

[1] Musial W, Ram B. Large-scale offshore wind power in the United States: assessment of opportunities and barriers. 2010. Golden, CO.
[2] Seidel M. Substructures for offshore wind turbines current trends and developments. 2014.
[3] Versteijlen W, Metrikine A, Hoving J, Smid E, de Vries W. Estimation of the vibration decrement of an offshore wind turbine support structure caused by its interaction with soil. In: EWEA offshore conference; 2011.
[4] Salzmann DJ, van der Tempel J. Aerodynamic damping in the design of support structures for offshore wind turbines. In: Paper of the Copenhagen offshore conference; 2005.
[5] Valamanesh V, Myers A. Aerodynamic damping and seismic response of horizontal axis wind turbine towers. J Struct Eng 2014;140:11.
[6] Tarp-Johansen NJ, Andersen L, Christensen E, Mørch C, Kallesøe B, Frandsen S. Comparing sources of damping of cross-wind motion. In: European offshore wind 2009: conference & exhibition; 14–16 September, 2009.
[7] Shirzadeh R, Devriendt C, Bidakhvidi M a, Guillaume P. Experimental and computational damping estimation of an offshore wind turbine on a monopile foundation. J Wind Eng Ind Aerodyn Sep. 2013;120:96–106.
[8] GL WindEnergie. Overall damping for piled offshore support structures, guideline for the certification of offshore wind turbines. Germanischer Lloyd WindEnergie; 2005.
[9] IEC 61400-3. Design requirements for offshore wind turbines. 2009. Brussels.

[10] DNV. DNV-OS-J101 design of offshore wind turbine structures. Det Norske Veritas AS; 2013.
[11] Damgaard M, Andersen J, I. LB, Andersen L. Time-varying dynamic properties of offshore wind turbines evaluated by modal testing. In: Proceedings of the 18th international conference on soil mechanics and geotechnical engineering; 2013. p. 2343–6.
[12] Petersen B, Pollack M, Connell B, Greeley D, Davis D, Slavik C, et al. Evaluate the effect of turbine period of vibrations requirements on structural design parameters. 2010. Groton, CT.
[13] Lombardi D, Bhattacharya S, Muir Wood D. Dynamic soil–structure interaction of monopile supported wind turbines in cohesive soil. Soil Dyn Earthq Eng Jun. 2013;49:165–80.
[14] Damgaard M, Andersen J, Ibsen LB, Andersen L. Natural frequency and damping estimation of an offshore wind turbine structure. Proceedings of the twenty-second international offshore and polar engineering conference, vol. 4; 2012. p. 300–7.
[15] Jonkman J, Butterfield S, Musial W, Scott G. Definition of a 5-MW reference wind turbine for offshore system development definition of a 5-MW reference wind turbine for offshore system development. 2009.
[16] ADINA. Watertown, MA: ADINA R&D, Inc.; 2014.
[17] Hansteen OE, Höeg K. Soil-structure interaction analysis of embedded caisson anchor under tension load. In: BOSS'94, 7th international conference on the behavior of offshore structures; 1994. p. 49–62.
[18] NGI. Description of INFIDEL – a non-linear, 3-D finite element program. 1991.
[19] Bush E, Manuel L. Foundation models for offshore wind turbines. In: 47th AIAA aerospace sciences meeting including the new horizons forum and aerospace exposition; 2009. no. January.
[20] Andersen LV, Vahdatirad MJ, Sichani MT, Sørensen JD. Natural frequencies of wind turbines on monopile foundations in clayey soils—a probabilistic approach. Comput Geotech Jun. 2012;43:1–11.
[21] Jonkman J, Buhl MJ. FAST user's guide. 2005. Golden, CO.
[22] Chopra AK. Dynamics of structures: theory and applications to earthquake engineering. 3rd ed. Upper Saddle River, NJ: Pearson Prentice Hall; 2007.
[23] Darendeli M. Development of a new family of normalized modulus reduction and material damping curves. Austin, TX: University of Texas at Austin; 2001.
[24] Carswell W, Arwade SR, Degroot DJ, Lackner MA. Probabilistic analysis of offshore wind turbine soil-structure interaction. University of Massachusetts Amherst; 2012.
[25] Goyal A, Chopra A. Simplified evaluation of added hydrodynamic mass for intake towers. J Eng Mech 1989;115(7):1393–412.
[26] Manwell JF, McGowan JG, Rogers AL. Wind energy explained. 2nd ed. New York: John Wiley & Sons, Ltd; 2009.